Composite Structures 347 (2024) 118451

Contents lists available at ScienceDirect

Composite Structures

journal homepage: www.elsevier.com/locate/compstruct

Failure analysis of unidirectional CFRP composites with the coupled effects of initial fibre waviness and voids under longitudinal compression

Jiayun Chen [a], Lei Wan [b,c,*], Katherine Nelms [c], Giuliano Allegri [c], Dongmin Yang [d]

[a] College of General Aviation and Flight, Nanjing University of Aeronautics and Astronautics, Nanjing 210016, China
[b] School of Engineering, University of Hull, Hull HU6 7RX, UK
[c] Bristol Composites Institute, University of Bristol, University Walk, Bristol BS8 1TR, UK
[d] Institute for Materials and Processes, School of Engineering, University of Edinburgh, Edinburgh EH9 3FB, UK

ARTICLE INFO

Keywords:
Unidirectional composites
Fibre kinking
Waviness angle
Void volume fraction
Void size

ABSTRACT

This research delves into the failure mechanisms exhibited by unidirectional Carbon Fiber Reinforced Polymer (CFRP) composites under longitudinal compression, while considering the interplay of three types of manufacturing-induced defects: initial waviness of fibres, void volume fraction, and void size. The study employs 3D high-fidelity intact representative volume element (RVE) models, incorporating the initial waviness of fibres and voids based on Micro-CT imaging. A novel algorithm is proposed to generate more accurate 3D void shapes, departing from conventional circular or triangular approximations. The results highlight the substantial influence of the initial waviness angle on the reduction of predicted compressive stiffness and strength. The volume and size of voids play a significant role in determining damage initiation within the composites. The failure mechanisms of the composite under the coupled effects of initial waviness of fibres and voids are discussed, exhibiting reasonable agreement with experimental observations.

1. Introduction

Carbon fibre-reinforced polymer (CFRP) composites are increasingly popular alternatives to replace traditional metallic counterparts due to their high specific properties and the capability of tailoring to achieve desired stiffness and strength in a specific direction [1,2]. The excellent longitudinal tensile properties are a selling point of composites, however, their longitudinal compressive strength is much smaller than the tensile strength, such as 62.1 % of the latter for unidirectional (UD) IM7/8552 CFRP composites [3]. Such a phenomenon jeopardises the safe performance of composite structures, severely limiting composites' application. The failure of composites is determined by the mechanical properties of fibres and matrix and the manufacturing-induced stochasticity and defects, such as the initial misalignment/waviness of fibres and voids in the matrix. Thus, it is crucial to understand the failure mechanisms of composites considering the existence of manufacturing-induced defects under longitudinal compression in order to maximise the potential of CFRP composites.

The formation, morphology analysis and the influences of voids on the mechanical properties under longitudinal compression are reviewed in [4], in which the 3D "needle-like" elongated and spherical voids were observed in the intra-laminar of composites using X-ray micro-tomography (micro-CT) with the volume fraction of voids less than 6 % [5]. It was found that the fibre-kinking phenomenon is not only related to the mechanical properties and geometrical characteristics of the fibres and matrix but also affected by the defects and initial waviness of fibres [6,7]. The previous experimental studies [8–13] indicated that the fibre kinking generally initiates at the regions with initial fibre misalignment/waviness, resulting in matrix plastic deformation due to the inter-fibre shear stress. The shear deformation, in return, aggravates the fibre rotation, further increasing the local shear stress. Such shear instability occurs when the shear stress reaches the shear yielding strength of the matrix and the shear damage mode transforms into the fibre kinking mode, contributing to the kink-band formation [11]. Other studies indicated that with a larger waviness angle, the fibre kinking is more likely to occur in composite materials, which contributes to the reduction of compressive failure strength drastically [14,15]. In addition, void formation in the thermoset composites is inevitable during the curing process of composites due to the infiltration between resin and fibre, the generation of volatile gas, curing pressure and other factors [16,17]. Therefore, it is important to consider the abovementioned uncertainties when predicting the failure strength of composites under

* Corresponding author at: School of Engineering, University of Hull, Hull HU6 7RX, UK.
E-mail address: l.wan@hull.ac.uk (L. Wan).

https://doi.org/10.1016/j.compstruct.2024.118451
Received 21 April 2024; Received in revised form 28 June 2024; Accepted 31 July 2024
Available online 5 August 2024
0263-8223/© 2024 The Author(s). Published by Elsevier Ltd. This is an open access article under the CC BY license (http://creativecommons.org/licenses/by/4.0/).

longitudinal compression.

Many theories have been proposed in order to establish the quantitative relationship between the macroscopic properties of composites and their microstructure, including defects. The widely used theoretical and numerical approaches for the investigation of the failure prediction of composites include the Eshelby equivalent inclusion theory [18,19], the Mori-Tanaka method [20] and the computational micromechanical methods [21–23]. Among those approaches, computational micromechanics offers a novel approach to understanding the deformation and fracture mechanisms in material engineering. Numerical simulations of representative volume elements (RVE) at the microscale level have been shown to be useful for predicting the mechanical properties of composite materials [24], which can provide the necessary input data for failure analysis at the mesoscale level. Moreover, the influences of the microstructure and material properties of constituents can also be addressed via parametric studies by means of the RVE modelling [25,26]. Regarding the failure analysis of composites under longitudinal compression, the 2D RVE model was an effective tool for the failure prediction of mechanical properties of CFRP composites. Pimenta et al. [9] investigated the influences of the constitutive models of constituents on the failure prediction of composites. It was found the constitutive model of the matrix has significant influences on the kink-band formation under longitudinal compression, and a linear-elastic-perfectly-plastic constitutive law was proved to be sufficient for accurate modelling. The sequence of events leading to fibre kinking was also proposed in the failure prediction of composites with the validation of experimental findings. Prabhakar and Waas [12] studied the interaction between fibre kink banding and splitting in unidirectional composites under longitudinal compression with a 2D micromechanical model. It was found that the compressive failure of composites was dominated by splitting and the compressive strength is significantly influenced by the shear strength of the interface between fibres and matrix.

With the significant improvement in computing power, in order to more accurately describe the effect of the microstructure on the mechanical behaviour of materials under compression, a high-fidelity 3D RVE model is a necessity. Naya et al. [27] measured the mechanical parameters of fibre and matrix under different environmental conditions and then analysed the fibre kinking mechanisms of unidirectional FRP composites under different environmental conditions using a 3D RVE model. In order to capture the realistic influence of the manufacturing-induced inevitable voids on the failure behaviour of composites, some studies took the size and distribution of voids into account in the micromechanical analysis. He et al. [28] investigated the failure mechanisms of unidirectional composites with various fibre radii, fibre shape deviations and matrix void content using a 2D RVE model under transverse loadings. Li et al. [29] studied the effect of void distribution on the transverse behaviour of unidirectional composites with a 2D RVE, in which the distribution and size of the voids are random. It was found the distribution of voids has a larger influence on the initiation and evolution of damage in the composites than the transverse stiffness and strength of the composites.

However, though the reviewed literature considers the influences of voids in micromechanical failure analysis, these studies mainly focus on the mechanical behaviour under transverse loading conditions or are limited to two dimensions. For the unavoidable defects, namely the initial waviness of fibres and voids in a matrix during manufacturing process, the study of the coupled influences of the initial waviness angle and voids on fibre kinking is undoubtedly a crucial topic for the accurate prediction of the mechanical properties of composites. Therefore, this paper focuses on the coupled influences of the initial waviness and voids on fibre kinking mechanisms in unidirectional CFRP composites using experimental and numerical approaches. Micro-CT was used to measure the initial waviness angle of fibres and the size and volume fraction of voids. Based on the experimental measurements, high-fidelity 3D RVE models, considering waviness and voids, were constructed to predict the failure strength of the composites under longitudinal compression. The RVE models, containing 50 fibres embedded in a matrix, were extended from our previous works [30–32], which has proved to be efficient in capturing the failure modes of matrix under transverse and in-plane shear loadings. In addition, the model in this study introduces fibre waviness and voids with weakening partial elements and considers the dispersity of voids size and distribution with randomisation and iterative algorithm.

The paper is organised as follows: the introduction is followed by the construction of computational micromechanics-based models which is discussed in Section 2, including 3D RVE models, the constitutive models of constituents and the definition of initial waviness and voids. The longitudinal compressive stiffness and strength of IM7/8552 composites with different waviness angles of fibres, volume fractions, and sizes of voids are predicted and validated in Section 3. A new method to measure the kink-band at peak load for 3D numerical simulations with random fibre distributions is proposed for characterising the relationship between the compressive strength and the matrix yielding within fibre kink-band region and the kink-band width and fibre rotation angle are predicted with the defects and discussed in Section 4. The coulped effects of the defects on the failure mechanisms are discussed in Section 5. Section 6 summaries the main conclusions.

2. Computational modelling of UD composites

2.1. 3D representative volume element model

The computational micromechanics-based model, considering initial fibre waviness and voids, was used to conduct the progressive failure analysis of a unidirectional composite under longitudinal compression. The RVE is defined as the smallest volume element which is large enough to represent the micro-structure of composites yet small enough for computation cost, the effective properties of a composite material correspond to properties averaged over a repeating RVE. Therefore, fibres in cross section area with periodic distribution are introduced in the models to reconcile the representativeness of RVE and the dispersity of fibres. The RVE model containing 50 fibres was found large enough to capture the essential features of the microstructural behaviour while maintaining reasonable computational cost [27,30,31,34]. The average fibre diameter is 7 μm with the fibre volume fraction was set to 60 % for the IM7/8552 [32]. The microstructure of the 2D RVE model was synthetically generated using a discrete element method-based algorithm which is statistically equivalent to the realistic fibre distribution [33]. In order to capture the influence of the initial fibre waviness angle in the formation of kink-band, the 2D RVE model was extruded along the fibre direction with a sinusoidal function to achieve the final 3D RVE, see Fig. 1. The fibres and matrix in the model were meshed using reduced integrated isoparametric linear wedge (C3D6) and brick (C3D8R) finite elements. The length of elements in the longitudinal direction is set to

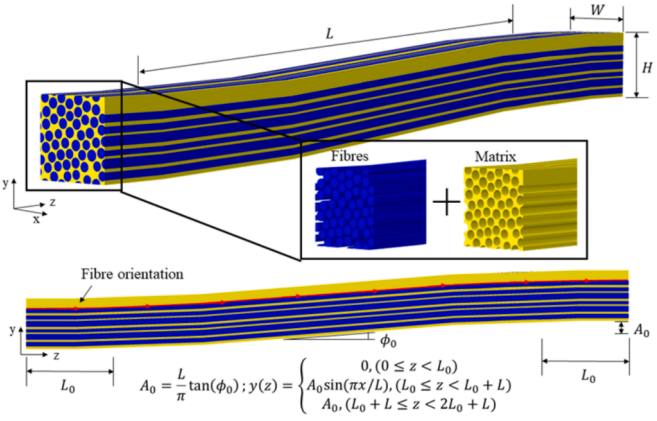

Fig. 1. 3D RVE model considering the initial fibre waviness.

approximately 6 μm, resulting in the total number of elements being 0.4 million. The main part of the RVE has an initial local fibre waviness equal to one-half of the wavelength (L=500 μm) associated with the sinusoidal function. Two straight parts ($L_0 = 50\ \mu m$) are added at both ends to eliminate the boundary effects on the formation of the kink-band. The dimensions of the cross-section are 50 $\mu m \times 50\ \mu m$. A local material orientation, which is the tangent direction corresponding to the sinusoidal-generated function, was used to assign the fibre direction in the ABAQUS.

Periodic boundary conditions are usually used for the failure analysis of RVE models to maintain the periodicity of stress and displacement fields, however, a significant growing of computational cost is needed due to excessive boundary constrains, especially for those who cannot access high-performance computing platforms. Gitman et al. [35] and Kereke et al. [36] conducted a study on the influences of boundaries on the prediction of elastic properties of composites. They found that the difference in the prediction obtained from the uniform boundary conditions and periodic boundary conditions ranges between 5–30 %. It was also reported in [26,34,37,38] that for the RVEs with more than 30 fibres embedded, the results obtained from periodic boundary conditions are close to those obtained from displacement or traction loading. For the models in this study, 50 fibres are embedded in RVEs, which is enough to capture accurate mechanical behaviours without periodic boundary conditions according to the literature aforementioned. Thus, in this study, uniaxial longitudinal compression was realised with fixing the transitional motions at the end surface with $z = 0$ and applying uniform z-direction displacement on the other end surface without constraining the translational motion in x and y directions, and the boundaries of other surfaces remain traction free and un-restrained.

2.2. Material models of constituents

The carbon fibres were modelled to be linearly elastic and transversely isotropic, which were defined with five independent elastic constants ($E_1, E_2, \upsilon_{12}, G_{12}, G_{23}$). The experimental findings exhibit brittleness under tension and extensive plastic deformation under compression and shear for the epoxy resin system [39]. Thus, the polymeric matrix in IM7/8552 composite materials was modelled by a Drucker-Prager plastic damage model [40], which is based on the yield function by Lubliner et al. [41] and modified by Lee and Fenves [42]. Under tension-dominated loadings, the quasi-brittle behaviour can be captured by the model with a damage variable. After the onset of damage, the softening behaviour is captured by an exponential cohesive model, characterized by the single normalized scaler damage variable. Thus, the correct fracture energy dissipation of the matrix G_m can be ensured. While for compression and/or shear-dominated loadings, the behaviour of the matrix is assumed to be perfect plastic. More details about the constitutive model and its numerical implementation in ABAQUS/Explicit refer to [40].

The fibre/matrix interface is usually modelled with a classical cohesive zone element to capture the interface debonding [22,30]. In order to capture the friction effect after interface failure under compression, a Coulomb friction law is coupled into the cohesive element via a VUMAT subroutine in ABAQUS. Considering the computational cost of the simulation of failure prediction in the longitudinal compression with the 3D high-fidelity RVE model, the interface was modelled using a surface-based frictional-cohesive zone model [27]. The cohesive interaction is governed by a traction-separation law. The damage onset is controlled by a quadratic stress criterion, which considers the damage modes, such as tension opening mode, shear mode and mix mode. The damage propagation is ruled by the Benzeggagh-Kenane law with a power exponent and critical energy release rates in pure modes (G_{IC}, G_{IIC}andG_{IIIC}). The isotropic Coulomb friction law, characterised by a friction coefficient μ, is coupled with the cohesive behaviour of the interface. Further details about the frictional-cohesive model can be found in [27,43]. The material properties of the constituents of IM7/8552 UD composites can be found in Table 1.

2.3. Definition of initial fibres waviness and voids

During the fabrication process of composite laminates, manufacturing-induced pore and void defects are inevitable due to insufficient resin infiltration. Pore defects usually refer to the voids close to the surface, however, an RVE model of composites represents the internal geometrical features, which are far away from the surface to avoid boundary effects. In RVE modelling, there are two strategies used to model voids in a matrix, a) deleting the matrix elements and b) weakening the matrix elements. It was reported that both strategies can achieve similar results regarding the prediction of mechanical properties of the composites [45]. In order to mitigate the risk of convergence issues, the second strategy was utilised by weakening the elements of matrix to represent the void defects, in which the elastic properties of voids elements are only 1 % of the other elements. The similar method was reported in the modelling of UD composites [45] and 3D woven composites [46].

The volume fraction of voids (f_v) is defined as V_{voids}/V_{RVE}, in which the V_{voids} is the volume of voids and the V_{RVE} is the volume of the whole RVE. Five RVE models with different voids volume fractions (1–5 %) are adopted in this study based on the experimentally determined volume fraction of voids (1.31–1.94 %, see Appendix) and the consideration of the maximum acceptable void fraction of 5 % in the engineering applications [16]. Although the shape of the realistic voids in composites is complex and varied, experimental images show that the shape of the voids in a composite with a low void fraction is elongated along the fibre direction [47], see Fig. 2. As such, our RVE models are constructed to further probe the effects of elongated voids commonly observed.

In order to investigate the influences of void sizes on the mechanical behaviour of composites under longitudinal compression, three void sizes, namely Type I (average size 4.37 μm^3), II (average size 75.50 μm^3) and III (average size 460 μm^3), were adopted, which can be found in the RVEs with $\Phi_0 = 5^\circ$, $f_v = 3$ %, see Fig. 3. In Fig. 3 regarding the voids of Type I, individual isolated voids are represented by a single element, which was randomly generated via a python script. It should be noted that the shape of elements is dependent on the mesh along fibre direction, which is slender in this study. Smaller elements could be achieved with a consequence of drastically increased computational cost. The voids of type II and III consist of multiple elements to construct larger voids while keep consistent volume fraction with a slight difference due to the shape of elements. Besides, due to the random distribution of the voids within an RVE, with the increase of void volume fraction and void size, voids could join together to form a larger void or align with fibres to represent the defects of fibre/matrix interface, see Fig. 4.

The flowchart of the generation of different types of voids in the RVE models is found in Fig. 5. For the generation of Type I voids, the number of voids N_{voids} is defined as $N_{voids} = V_{voids}/V_{AVE}$, where V_{AVE} is the average volume of void elements. Then the number of void elements in the matrix was selected randomly as a void set. For the generation of Type II voids, an "anchor element" was introduced, which was randomly

Table 1
Material properties of the constituents of IM7/8552 composite and identified interface parameters [3,30,32,44].

IM7 fibre properties					
E_1 (GPa)	$E_2 = E3$ (GPa)	ν_{12}	ν_{23}	G_{12} (GPa)	G_{23} (GPa)
287	13.399	0.29	0.48	23.8	7

8552 epoxy properties				
E (GPa)	ν_m	σ_{myt} (MPa)	σ_{myc} (MPa)	G_m (J/m^2)
4.08	0.38	99	130	100

Contact properties at fibre/matrix interface				
$K_{nn} = K_{ss} = K_{tt}$ (GPa/mm)	t_{0n} (MPa)	$t_{0s} = t_{0t}$ (MPa)	G_{IC} (J/m^2)	$G_{IIC} = G_{IIIC}$ (J/m^2)
10^6	58	92	2	100

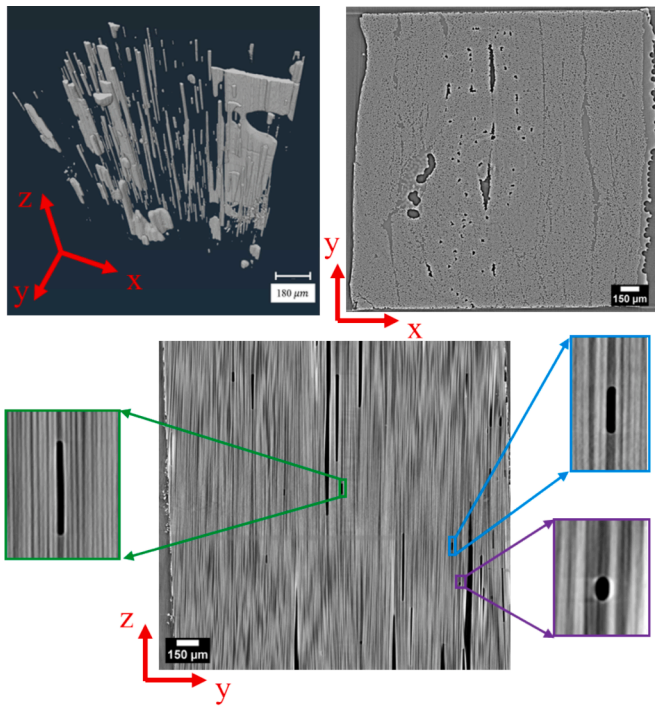

Fig. 2. Tomograph and CT slices taken of UD CFRP samples manufactured and described in [48] (top left) voids segmented from a representative sample (top right) XY slice showing void cross sections and (bottom) a representative XZ slice demonstrating different types of voids present within samples made using the methods in [48].

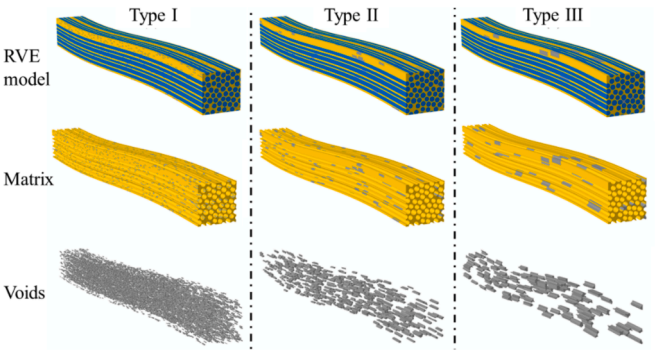

Fig. 3. Three types of void size type I, type II and type III in 3D RVE models with $\Phi_0 = 5°$, $f_v = 3$ %.

generated for the construction of larger voids. The number of "anchor elements" in Type II is defined as $N_{AE}=V_{voids}/3^3V_{AVE}$. The 27 elements which share the same nodes with the "anchor elements" were selected as a void set. While for the generation of Type III voids, in order to generate the larger voids more efficiently, an "anchor node" was introduced. The number of nodes is defined as $N_{AN}=V_{voids}/6^3V_{AVE}$, in which the nodes were generated randomly. The 8 elements which share the same node were selected as the "anchor elements". This process was repeated twice, resulting in the construction of a void set consisting of 216 elements. For all three strategies, the target volume fraction of voids V_{voidsA} can be computed by summing up the volume of each void set. The generation of voids is completed once the difference between the V_{voids} and V_{voidsA} is less than 5 %.

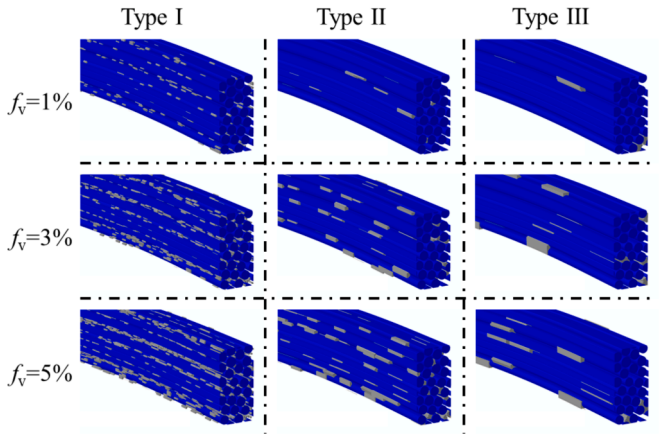

Fig. 4. Various void morphology (Type I, Type II and Type III) in RVE models with different void volume fractions f_v = 1 %, 3 % and 5 %. Voids are in grey while fibres are in blue, and voids are in alignment with fibres due to the shape of elements.

3. The influences of coupled waviness and voids on longitudinal compressive stiffness and strength

3.1. Longitudinal compression stiffness

In this study, three parameters are selected for the study of their influences on predicted longitudinal compressive stiffness of IM7/8552 composites: initial waviness angle of fibres, the volume fraction and the size of voids. Table 2 lists the predicted stiffness of the composites with the consideration of the abovementioned three parameters compared with the one obtained from "intact" (voids-free) RVE models. In order to reduce the computational cost, the influences of void size on the failure prediction were conducted on the RVE models with the initial fibre waviness angle of 1°, 3° and 5°. It was observed from simulated compression that the longitudinal compressive stiffness decreases as the initial waviness angle of fibres increases for both the intact models and the models with voids. The stiffness decreases by around 10 % when the angle reaches 5° for the intact model, which can be found in Fig. 6. This is mainly due to the bending of fibres under longitudinal compression, caused by the initial waviness of fibres [49]. However, little difference is observed in the prediction obtained from the models with different volume fractions and types of voids. This is mainly because the longitudinal stiffnesses of composites are largely dependent on the longitudinal stiffness of fibres, according to the rule of mixture.

3.2. Longitudinal compressive strength

In order to understand the effects of manufacturing-induced defects on the longitudinal compressive strength of composites, the strength is predicted on the RVE models with the combinations of three variations. Table 3 lists the predicted failure strength of IM7/8552 composites under longitudinal compression considering the initial waviness angle of fibres, the volume fraction and size of voids. It can be found that the initial angle has significant influences on the failure strength of composites, *i.e.*, the strength decreases by around 29 % when the angle increases from 1° to 3°, which is in a good agreement with the experimental findings of 33 % reduction in compressive strength with angle increasing from 1.2° to 3.2° [50]. It should be noted that the failure strength of the composites with an initial waviness angle of 1° is 25–50 % larger than the experimental longitudinal compressive strengths (X_{11} = 1.2–1.45 GPa) [51,52]. This discrepancy is attributed to that the failure mechanism of composites with an initial waviness angle of fibres not larger than 1° under longitudinal compression is fibre crushing, which is governed by fibre compressive strength [27].

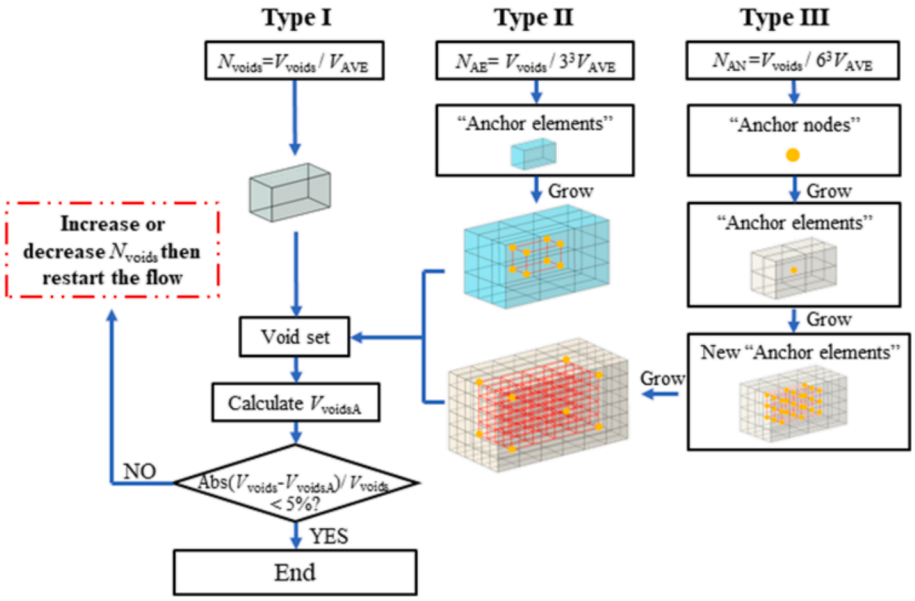

Fig. 5. The flow chart of the realization of different void sizes in the RVE model.

Table 2
Comparison between predictions of Young's Modulus of CFRP composites with different voids and initial waviness angles under longitudinal compression (units: GPa).

Φ_0	Intact model	Void volume										
		1 %			2 %	3 %			4 %	5 %		
		Void size										
		I	II	III	I	I	II	III	I	I	II	III
1°	172.23	172.23	172.38	172.28	172.13	172.1	172.05	172.1	172.05	171.97	171.99	172.14
2°	170.36	170.17	–	–	170.24	170.19	–	–	170.12	170.06	–	–
3°	167.28	167.14	167.34	167.18	167.1	167.06	167.02	167.05	167	166.92	166.98	167
4°	162.91	162.91	–	–	162.69	162.6	–	–	162.63	162.45	–	–
5°	157.91	157.85	157.8	157.79	157.7	157.61	157.56	157.56	157.52	157.43	157.4	157.28

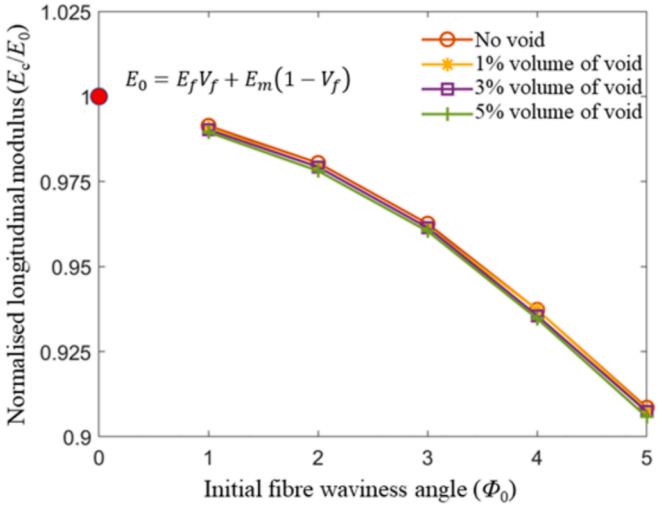

Fig. 6. Predicted longitudinal compression modulus of IM7/8552 with Type-I voids, different voids volumes and fractions for different initial waviness angles of fibres.

However, when the angle is beyond 1°, the failure is controlled by the initial fibre waviness angle and matrix plasticity, resulting in the formation of a kink-band [27,53]. The predicted strengths are shown in Fig. 7 and compared against experimental results of IM7/8552 samples tested under longitudinal compression according to ASTM D3410 [52]. Notably, the experiments did not include the measurement of initial fibre waviness angle or void content. With this in mind, the predicted strengths of the composites with the initial waviness angle of fibres between 1.3–2.4° fall within the experimental range reported by [51,52].

Three sizes of voids, Type I, II and III, are considered for the failure prediction of composites with three void volume fractions ($f_v = 1$ %, 3 % and 5 %.) and three initial waviness angles ($\Phi_0 = 1°$, 3° and 5°). It can be found that in all the combinations, with the increase of void size from Type I to Type III, the failure strength decreases. This is because with a larger void in the matrix, stress wave propagation is block by the void which initiates stress concentration around the void. When the initial waviness angle is 3°, with the increase of the volume fraction of voids, the reduction of failure strength from Type I to Type III increases from 0.18 % at $f_v = 1$ % to 1.5 % at $f_v = 5$ %. Interestingly, when the volume fraction of voids is 3 %, the reduction of failure strength decreases from 1 % at $\Phi_0 = 1°$ to 0.37 % at $\Phi_0 = 5°$. This suggests that the initial waviness angle of fibres has larger influences on failure strength compared to the void size.

For Type I voids, there is only 1.54–1.86 % reduction in strength between the model with the highest volume fraction 5 % of voids compared to the intact model for each initial waviness angle of fibres (see Fig. 7). For composites with an initial waviness angle larger than 1°, the failure strength is determined due to the shear-driven failure of the matrix [53,54]. According to the results obtained from the simulations where the initial waviness angle of fibres ranges from 2° to 5°, the volume fraction of Type I voids has slight influences on the failure

Table 3
Comparison between predictions of the strength of CFRP composite with different voids and waviness angles under longitudinal compression.

φ_0	Intact model	Void volume										
		1 %			2 %	3 %			4 %	5 %		
		Void size										
		I	II	III	I	I	II	III	I	I	II	III
1°	1545.35	1538.61	1536.34	1535.44	1532.92	1526.56	1519.57	1511.81	1520.23	1511.12	1491.98	1487.20
2°	1297.71	1292.37			1287.61	1282.93			1277.35	1271.65		
3°	1101.53	1098.03	1096.58	1096.92	1094.62	1090.54	1087.38	1083.78	1086.17	1081.68	1073.49	1070.26
4°	935.76	933.31			930.38	927.17			924.11	920.52		
5°	807.6	805.17	803.60	802.94	801.65	798.73	796.33	795.58	795.78	792.21	789.05	783.62

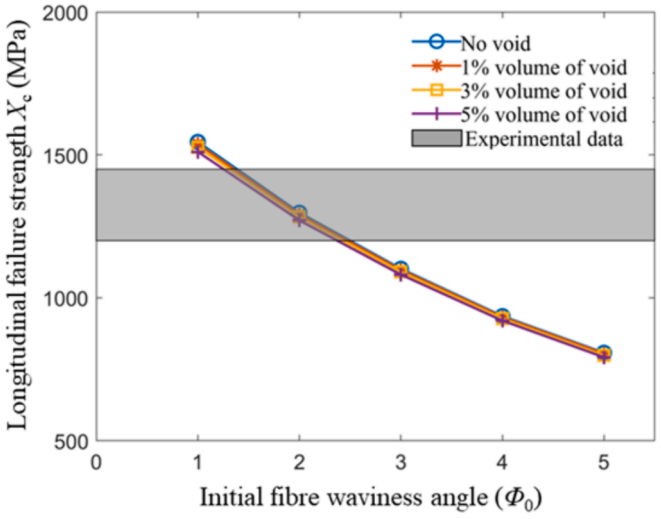

Fig. 7. Comparison of predicted failure strengths under longitudinal compression considering Type-I voids between numerical simulations and previously reported experimental data [51,52].

strength of composites. This is due to the fact that the damage initiation in the matrix usually occurs due to stress concentration caused by the voids.

4. The influences of coupled waviness and voids on the kink-band width and fibre rotation angle at peak load under longitudinal compression

4.1. Definition of the width of kink-band and fibre rotation angle at peak load

It is paramount to define the width of the kink-band and fibre rotation angle for the quantitative progressive failure analysis of composites under longitudinal compression from the numerical simulation point of view. Naya et al. [27] selected the plastic equivalent strain (PEEQ) at the surface of the RVE model to define the width of the kink band for the illustration of the damage evolution in the composites under longitudinal compression. However, this may not be appropriate due to the randomly distributed fibres embedded into matrix, which results in the different stress states at different locations of cross-section across the model width. Therefore, in order to characterise the relationship between the compressive strength and the matrix yielding within fibre kinking region, the length of the matrix shear yielding region at different locations of the cross-section across width was used to measure the kink-band width at peak load. Fig. 8 shows the definition of the kink-band width w_S and fibre rotation angle Φ in the numerical simulation of the RVE model with an initial waviness angle $\Phi_0 = 3°$ and Type I voids with $f_v = 3$ % at the peak load under longitudinal compression based on in-plane shear stress distribution. Due to the randomly distributed fibres in cross-section of the RVE, three planes A, B and C, which segment the RVE model into four parts equally along transversal direction, are selected to measure the kink-band width. Thus, the overall kink-band width w_S of the RVE based on shear stress regions can be defined as:

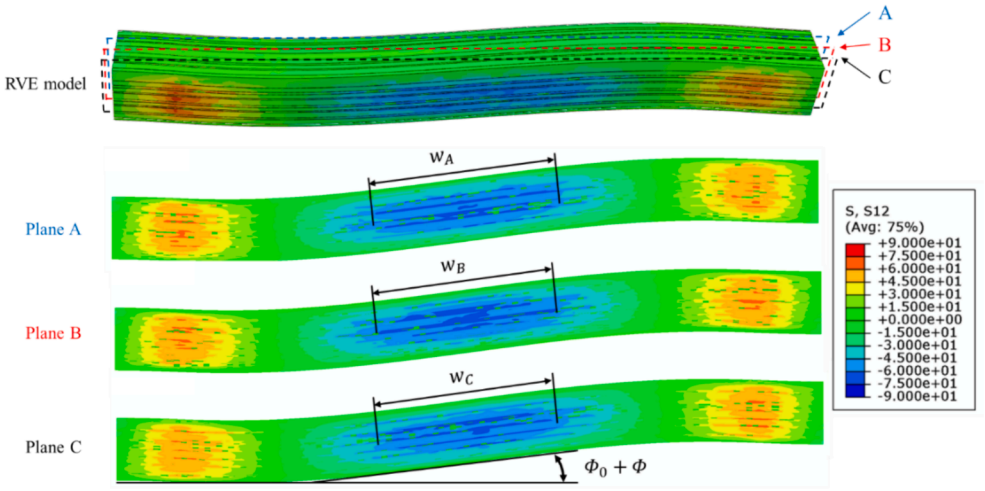

Fig. 8. Definition of the kink-band width w and fibre rotation angle Φ at the peak load from the numerical simulation of the RVE model with $\Phi_0 = 3°$, and Type I voids with $f_v = 3$ %. (Plane A, B and C represent three planes located at three different positions. Plane B is the central plane, and planes A and C are two symmetrical planes.).

$$w = \frac{w_A + w_B + w_C}{3}$$

where w_A, w_B and w_C are the kink-band width at planes A, B and C, respectively. The widths were determined based on the edges of the shear yielding regions. The rotation angle of fibres Φ can be defined in any of these planes.

4.2. Influences of initial waviness and voids on the formation of kink-band

Table 4 lists the predicted widths of the in-situ kink-band obtained from the shear plastic region (w_S) of the matrix at the peak load considering the initial waviness angle, and the shape and volume fraction of voids. When the initial waviness angle $\Phi_0 = 1^\circ$, no obvious kink band was observed from both regions. This is because up to $\Phi_0 = 1^\circ$, the failure mechanism is fibre crushing, which is governed by fibre compressive strength; while for the cases with the initial waviness angle above 1°, the failure of the RVE is controlled by the angle and matrix plasticity, resulting in the formation of kink-band [27,53]. It can be found in Table 4 that the kink-band width increases as the initial waviness angle increases. When increasing the volume fraction of voids from 1 % to 5 % with $\Phi_0 = 2^\circ$ and type I voids, the width of the kink-band increases by 35.5 %. However, the width only increases by 5.3 % when Φ_0 reaches 5 %, suggesting that the dominant factor influencing the predicted width is the initial waviness angles.

With the comparison of predicted widths of kink-band in different cases with the types of voids, it can be found that the width increases as the size of voids increases. Though, this trend was not always consistently observed due to the random distribution of voids. As a result, different cross sectional slices yielded different kink-band widths for the same simulated condition. Overall, the kink-band widths at peak loads obtained from the numerical simulation considering initial waviness and voids ranges between 85.76 and 174.99 μm. These band widths are in excellent agreement with the experimental findings that the kink-band is in the order of 10–30 fibre diameters [27,54], which is 70–210 μm in this study.

Table 5 lists the predicted final rotation angle (Φ) of fibres with different initial waviness angles and different volume fractions and types of voids. A 41 % reduction in the predicted rotation angle of fibres is found from intact RVE models as the initial waviness angle is increased from 2 to 5°, indicating the significant influences of the initial angle on the final rotation angle. This is because with the increase of the prescribed initial waviness angle, fibres tend to be vulnerable to bend [49], resulting in further bending with a similar compressive strain. A similar trend can also be found in other cases with the consideration of voids. Small fluctuation in the predicted rotation angle of fibres is found when comparing different cases considering the influences of volume fraction and type of voids. The whole range of the angle considering initial waviness and voids lies in 4–10.43°, which is in a reasonable agreement with the numerical and experimental findings [27].

5. The influences of coupled waviness and voids on failure mechanisms under longitudinal compression

5.1. Progressive failure analysis considering fibre waviness and voids

It was reported experimentally and numerically [6,10,11] that the fibre kinking failure in longitudinal compression was induced by shear yielding of matrix due to the initial waviness of fibres. In this study, two competing failure mechanisms were found in the intact numerical models: matrix tensile failure (splitting) and shear yielding. When the voids are introduced into the models, premature failure occurs due to stress concentration/rearrangement alongside voids where damage initiates and propagates by linking up the matrix cracks, resulting in the final failure with the kink-band containing primary cracking path discussed below.

As a representative example, Fig. 9 shows key numerical results obtained for two models with the sample waviness angle and different void contents. The first model is the intact RVE with $\Phi_0 = 3^\circ$ and the second is the RVE with $\Phi_0 = 3^\circ$, $f_v = 3$ % and type III voids. There are selected for the discussion about the effects of voids on the progressive failure analysis of composites under longitudinal compression. In the early stage before failure at point A in Fig. 9(a), the transverse and in-plane shear stress concentration (σ_2 and τ_{12}) are observed around voids tip, as shown in Fig. 9 (b) and (c), respectively. Micro cracks initiate from these voids and propagate along the voids longitudinal direction, resulting in matrix cracking and fibre/matrix interface debonding, see Fig. 9(d-e). This cracking and debonding indicates the failure of matrix and interface at post-failure point B. When fibres are no longer constrained by the matrix, they rotate until they can no longer bear the load in their severely rotated state. The fibres at this point fracture, and the kink-band forms, which is associated with matrix splitting.

For the composite without voids, evenly distributed and smaller stresses are found in the kink-band region at point A compared to the composite with voids, see Fig. 9(b-c). These features result in smooth transfer of stresses at the kink-band region and give rise to a smaller damage region compared to the model with voids, see Fig. 9(d) and (e) for matrix cracking and interface debonding, respectively. The comparison between the numerical results from the RVE models with and without voids suggest the voids expedite and aggravate stress concentration as well as matrix and interface damage, leading to an earlier failure and a slightly smaller failure strength, which can be found in the stress–strain curves in Fig. 9(a).

Finally, similar post-failure features can also be observed from the post-mortem X-Ray CT images of representative CFRP sample from [48], shown in Fig. 10. Due to the randomly distributed voids and aligned long fibres, the kink-band widths obtained in the experiments and predicted by the numerical simulations at peak load from different cut planes present to be different. Variation in the failure along the through thickness direction in both model and experimental samples highlights the necessity of 3D measurement which can be achieved using CT or with high fidelity models proposed herein.

Table 4
Comparison of predicted the kink-band width of fibres at peak loads under longitudinal compression.

Φ_0	Intact model		Void volume										
			1 %			2 %	3 %			4 %	5 %		
			Void size										
			I	II	III	I	I	II	III	I	I	II	III
1°	—	—	—	—	—	—	—	—	—	—	—	—	—
2°	w_S	75.22	85.76			92.98	105.27			116.17	121.23		
3°	w_S	97.84	103.55	104.14	102.04	108.72	122.54	125.12	131.47	134.25	136.38	138.25	156.73
4°	w_S	132.82	135.78			143.37	149.2			154.12	160.45		
5°	w_S	143.4	150.57	148.86	149.75	159.04	158.17	159.95	173.07	171.82	158.59	174.99	169.93

Table 5
Comparison of the predicted rotation angle (Φ) of fibres under longitudinal compression.

Φ_0	Intact model	Void volume										
		1 %			2 %	3 %			4 %	5 %		
		Void size										
		I	II	III	I	I	II	III	I	I	II	III
1°	4.27	4.61	4.00	4.55	4.22	4.44	4.09	4.40	4.01	4.05	4.33	3.84
2°	7.48	7.18			7.16	6.99			7.14	7.02		
3°	8.64	7.81	7.63	7.98	7.86	8.11	8.25	7.98	8.08	8.02	8.05	7.75
4°	9.13	8.92			9.03	8.87			9.13	9.10		
5°	10.52	10.24	10.23	10.00	10.12	10.37	10.5	10.26	10.17	10.12	10.43	10.11

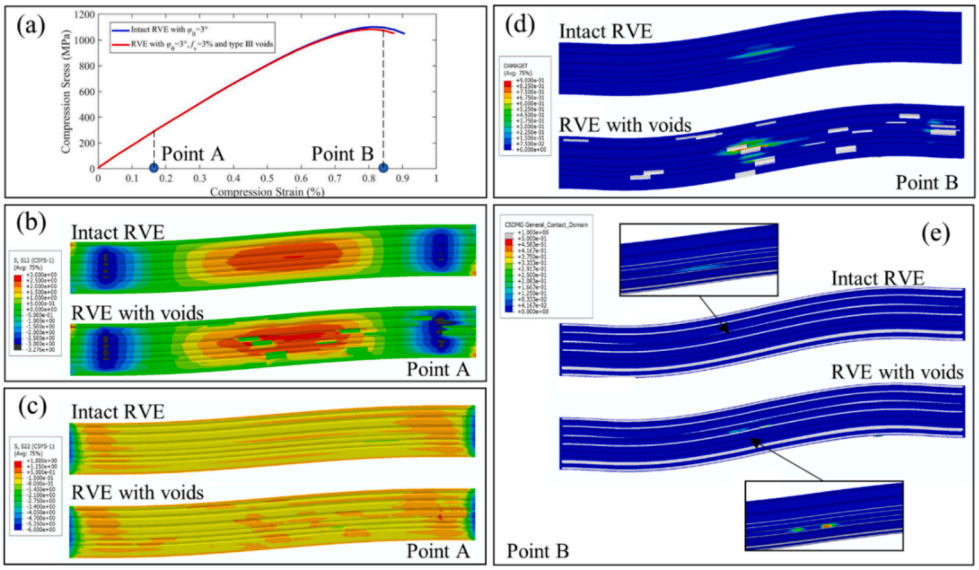

Fig. 9. Numerical results of the Intact RVE with $\Phi_0 = 3°$ and the RVE with $\Phi_0 = 3°, f_v = 3$ % and type III voids. (a) Stress–strain curve for both models. (b) In-plane shear stress concentration in both models at point A. (c) Transverse stress concentration in both models at point A. (d) Matrix splitting damage in both models at point B. (e) Fibre/matrix interface debonding damage in both models at point B.

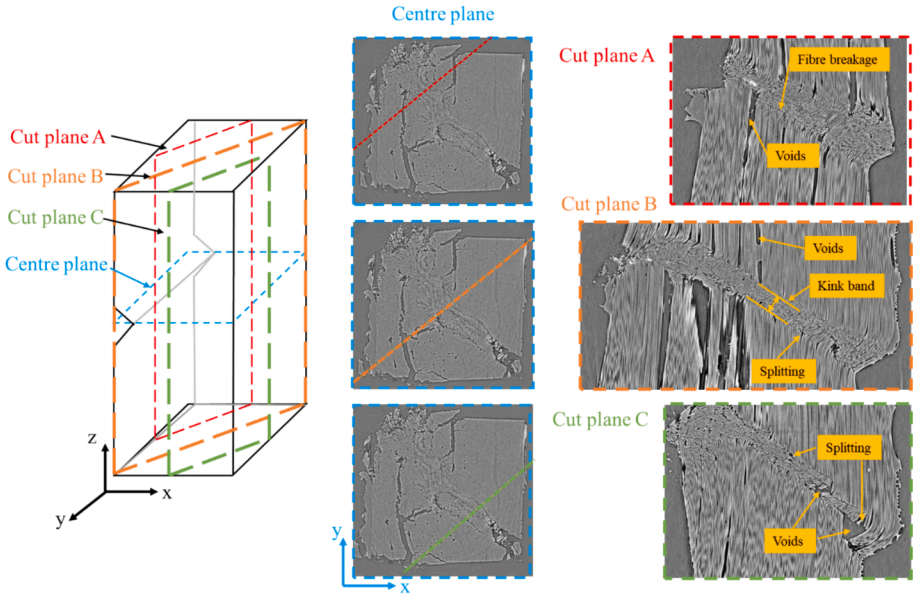

Fig. 10. Post-mortem X-Ray CT images of representative sample from [48] showing the geometry of kink-band at different cut planes. The cut planes are orientated parallel to the plane of the kink-band.

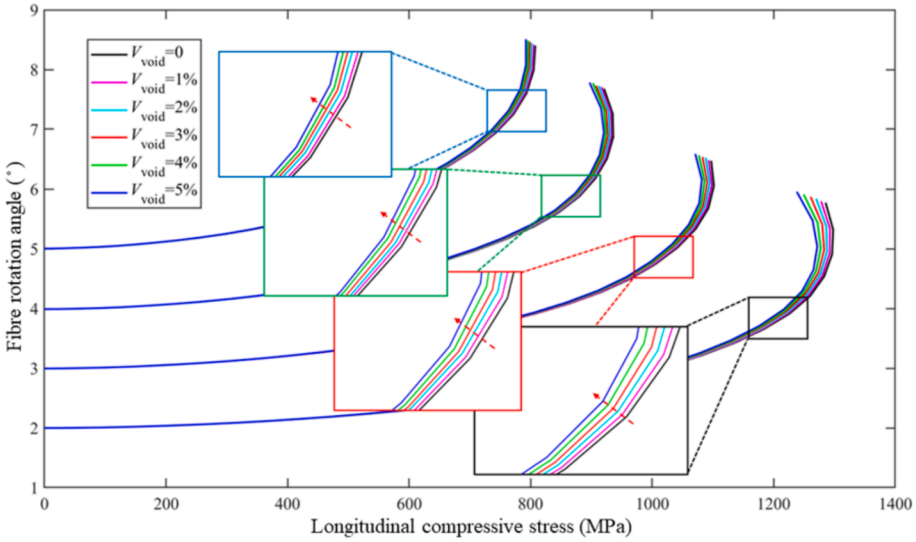

Fig. 11. Variation in compressive stress and final fibre rotation angle for different volume fractions of Type-I voids.

Fig. 11 presents the comparison of compressive stress and fibre rotation angle (Φ) considering different volume fraction of Type-I voids. An initial waviness angle of fibres was recorded when the compressive load is zero. Nearly linear lines at low or even moderate compressive stresses can be found which indicates the compressive load is mainly held by the fibres. With a small initial waviness angle of 2°, the reduction in compressive failure strength is larger with an increase of volume fraction of voids compared to the reduction in strength for the case of an initial waviness angle of 5°. This is mainly because with a larger prescribed initial waviness angle, fibres tend to be vulnerable to bend, resulting in faster failure. This suggests that the initial waviness angle plays a dominant role in the compressive failure compared to the voids.

5.2. *The influences of initial fibre waviness and voids on the failure mechanisms of composite*

Fig. 12 shows the influences of the initial waviness angle on the failure of composites and the kink-band formation with f_v = 3 % and Type I voids at the peak load. Matrix cracking or splitting indicated with the variable DAMAGET and matrix yielding indicated with shear stress S12 at the centre plane B (see Fig. 8) are used for the discussion of composite failure. It is found that when the initial waviness angle is 2°, both matrix cracking and longitudinal splitting can be found at the transitional region and kink-band, respectively. These damage features are often observed experimentally using in-situ or post-mortem techniques. For example, splitting at the transitional regions can be observed with Micro-CT at Cutting plane B in Fig. 10 as well as in-situ observation with the SEM in [54], which is mainly due to the difference between the bending stiffness of straight and curved parts. When the angle increases to 5°, matrix cracking and yielding disappear at the transitional region since the stress localisation mainly occurs in the centre of the RVE model where the kink-band is formed. Severe matrix cracking and plastic yielding are predicted in the kink-band region when the initial waviness angle reaches 3°, while the highly stressed kink-band region shrinks with the increase of angle. This is mainly due to the fact that the composite with a larger initial waviness angle such as 5° fails at a smaller strain of 0.68 % compared to 0.95 % for 1° and 0.83 % for 3°, resulting in not enough time for the highly stressed region to expand.

The influence of the volume fraction of Type I voids on the final failure of composites with Φ_0 = 3° under longitudinal compression is shown in Fig. 13. As the volume fraction increases, the damaged and highly stressed parts in splitting and kink-band regions, respectively, become discrete from continuous due to the existence of voids. When the volume fraction reaches f_v = 5 %, an interesting phenomenon can be captured in the DAMAGET field that the damage in the matrix initiates from the voids and propagates along the path parrel to the central line of the kink-band, linking the damages in the matrix and fibre/matrix interface.

Fig. 14 shows the influences of void size on the failure of composites with Φ_0 = 3° and f_v = 3 %. Compared to the kink-band at peak load obtained from the intact model, the void size has insignificant influence on the morphology of kink-band regions. However, when the size of voids increases from Type I to Type III, the locally damaged and highly stressed regions move associated with the location of the larger voids,

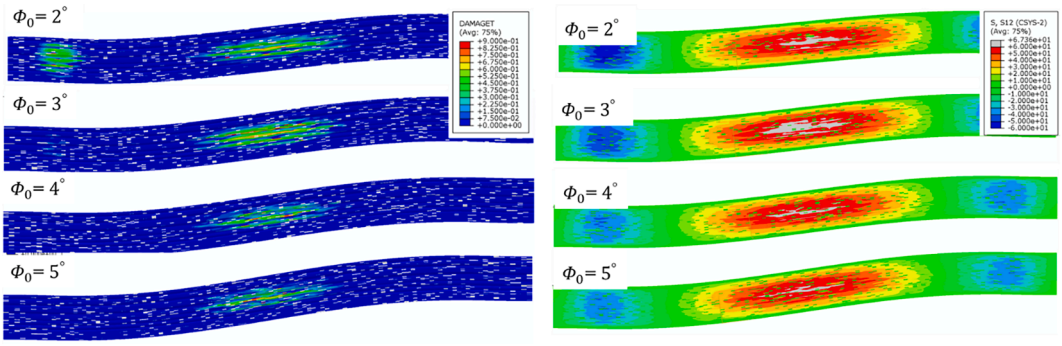

Fig. 12. Influences of the initial waviness angle on the failure of composites with f_v = 3 % and Type I voids and the images are taken from middle plan B (Left: Tensile damage distribution, which indicts matrix cracking. Right: In-plane shear stress distribution in the matrix, which indicates matrix plastic yielding).

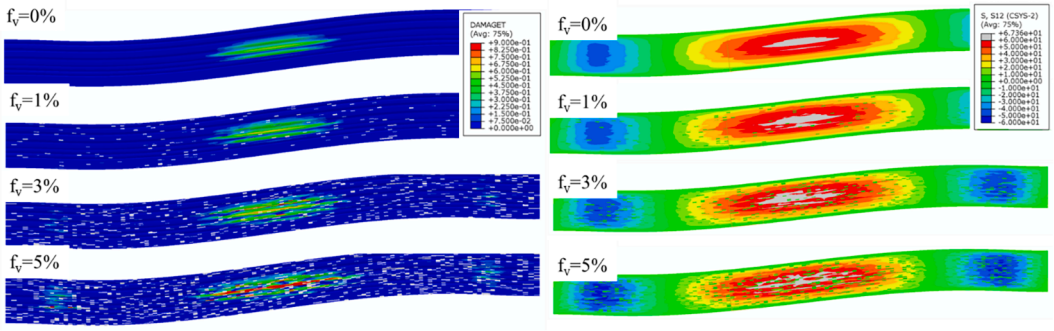

Fig. 13. Influences of the volume fraction of voids on the failure of composites with $\Phi_0 = 3^\circ$ and Type I voids and the images are taken from middle plan B (Left: Tensile damage distribution, which indicts matrix cracking. Right: In-plane shear stress distribution in the matrix, which indicates matrix plastic yielding).

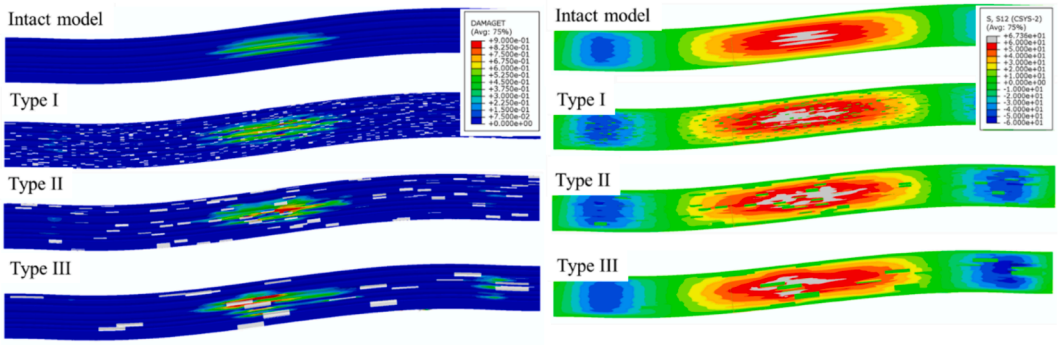

Fig. 14. Influences of the type of voids on the failure of composites with $\Phi_0 = 3^\circ$ and $f_v = 3$ % and the images are taken from middle plan B (Left: Tensile damage distribution, which indicts matrix cracking. Right: In-plane shear stress distribution in the matrix, which indicates matrix plastic yielding).

resulting in splitting and matrix yielding locally. Such voids-induced splitting phenomenon can also be observed from CT scanned images at Cutting plane C in Fig. 10.

6. Conclusion

This study investigated the influences of initial waviness of fibres and manufacturing-induced voids on the mechanical performance of unidirectional CFRP composites under longitudinal compression. 3D high-fidelity RVE models were generated based on the experimentally determined volume fraction of voids and void geometry as observed in Micro-CT tomographs of small UD CFRPs. A novel algorithm was developed to account for more these realistic 3D shapes of voids, instead of simplified circular or triangular shapes. The nonlinear mechanical behaviour of matrix was simulated using a pressure-dependent plastic damage Drucker-Prager model while the fibre/matrix interface debonding was modelled with cohesive-frictional interaction.

The novelty of this study includes:

- Realistic experimentally-determined void morphology was modelled with 3D high-fidelity micromechanics-based RVEs for the investigation of coupled initial waviness of fibres and voids on the progressive failure mechanisms of composites.
- An efficient algorithm was developed for the generation of voids by weakening the elements of matrix.
- A new method to measure the kink-band at peak load is proposed to characterise the relationship between the compression strength and the matrix yielding within fibre kink-band region.

The numerical results are compared to experimental findings and to key experimental results in the literature. The main conclusions are as follows:

- The initial waviness angle of fibres has significant influence on the longitudinal compressive modulus and strength for intact models, which decrease by 9.1 % and 52 % as the angle increases from 1° to 5°, respectively. However, the volume fraction and size of voids have smaller effects (~1.7 %) on the longitudinal compressive modulus and strength.
- The predicted kink-band width at peak load increases as the initial waviness angle and volume fraction of voids increase, while no obvious trend could be found in the effects of the void size on the predicted width. The fibre rotation angle increases as the initial waviness angle increases, while no obvious trend could be found in the effects of the volume fraction and size of voids.
- When the initial waviness angle of fibres is less than 1°, the failure of composites is dominated by fibre failure. While with the angle of larger than 1°, the damage initiated in the region where voids exist. As the angle increases, the highly stressed region moves from both ends towards the centre. The volume fraction and size of voids have detrimental effects on the damage initiation in matrix, and the damage propagates by linking the void regions where stress concentration occurs. The failure of composites is triggered by the matrix tensile damage in the form of splitting, which was observed in the Micro-CT scanned experimental images.

This investigation offers valuable insights into the complex failure behaviour of unidirectional CFRP composites, shedding light on the impact of manufacturing-induced defects on their mechanical performance. The developed 3D RVE models, along with the proposed algorithm and approaches, pave the way for more accurate and realistic simulations in the field of composite materials. Moreover, the outcomes emphasize the significance of controlling initial waviness and void-related defects to enhance the structural integrity and durability of CFRP composites in practical applications. It should also be noted that

the RVE models can mainly apply to the simulations for shear/splitting-driven composite failure under longitudinal compression where the manufacturing-induced defects, *i.e.*, initial waviness of fibres and voids, play a significant role. The fibre breakage under longitudinal compression will be tackled in our next study regarding the influence of fibre trajectory on the composite failure. In addition, due to the numerical convergence of the current RVE models, the simulation terminated soon after it reached peak load, thus the kink-band broadening could not be captured, which is our ongoing research with the consideration of fibre breakage under longitudinal compression.

CRediT authorship contribution statement

Jiayun Chen: Writing – original draft, Visualization, Investigation, Formal analysis, Data curation. **Lei Wan:** Writing – review & editing, Writing – original draft, Visualization, Validation, Supervision, Methodology, Investigation, Formal analysis, Conceptualization. **Katherine Nelms:** Writing – review & editing, Writing – original draft, Visualization, Software, Data curation. **Giuliano Allegri:** Writing – review & editing, Supervision. **Dongmin Yang:** Writing – review & editing, Supervision.

Declaration of competing interest

The authors declare that they have no known competing financial interests or personal relationships that could have appeared to influence the work reported in this paper.

Data availability

Data will be made available on request.

Appendix A. Supplementary material

Supplementary data to this article can be found online at https://doi.org/10.1016/j.compstruct.2024.118451.

References

[1] Das TK, Ghosh P, Das NC. Preparation, development, outcomes, and application versatility of carbon fiber-based polymer composites: a review. Adv Compos Hybrid Mater 2019;2:214–33. https://doi.org/10.1007/S42114-018-0072-Z/METRICS.

[2] Zhang J, Zhou P, Guan C, Liu TQ, Kang WH, Feng P, et al. An ultra-lightweight CFRP beam-string structure. Compos Struct 2021;257:113149. https://doi.org/10.1016/J.COMPSTRUCT.2020.113149.

[3] Kaddour AS, Hinton MJ, Smith PA, Li S. Mechanical properties and details of composite laminates for the test cases used in the third world-wide failure exercise. J Compos Mater 2013;47:2427–42. https://doi.org/10.1177/0021998313499477.

[4] Mehdikhani M, Gorbatikh L, Verpoest I, Lomov SV. Voids in fiber-reinforced polymer composites: a review on their formation, characteristics, and effects on mechanical performance. J Compos Mater 2019;53:1579–669.

[5] Yang P, Elhajjar R. Porosity content evaluation in carbon-fiber/epoxy composites using X-ray computed tomography. Polym Plast Technol Eng 2014;53:217–22. https://doi.org/10.1080/03602559.2013.843700.

[6] Bishara M, Rolfes R, Allix O. Revealing complex aspects of compressive failure of polymer composites – Part I: fiber kinking at microscale. Compos Struct 2017;169:105–15. https://doi.org/10.1016/J.COMPSTRUCT.2016.10.092.

[7] Bergan AC, Herráez M, González C, Lopes CS. A constitutive model for fiber kinking: formulation, finite element implementation, and verification. Compos Part A Appl Sci Manuf 2020;129:105682. https://doi.org/10.1016/J.COMPOSITESA.2019.105682.

[8] Pimenta S, Gutkin R, Pinho ST, Robinson P. A micromechanical model for kink-band formation: Part II—analytical modelling. Compos Sci Technol 2009;69:956–64. https://doi.org/10.1016/J.COMPSCITECH.2009.02.003.

[9] Pimenta S, Gutkin R, Pinho ST, Robinson P. A micromechanical model for kink-band formation: Part I — experimental study and numerical modelling. Compos Sci Technol 2009;69:948–55. https://doi.org/10.1016/J.COMPSCITECH.2009.02.010.

[10] Bai J, Phoenix SL. Compressive failure model for fiber composites by kink band initiation from obliquely aligned, shear-dislocated fiber breaks. Int J Solids Struct 2005;42:2089–128. https://doi.org/10.1016/J.IJSOLSTR.2004.08.011.

[11] Narayanan S, Schadler LS. Mechanisms of kink-band formation in graphite/epoxy composites: a micromechanical experimental study. Compos Sci Technol 1999;59:2201–13. https://doi.org/10.1016/S0266-3538(99)00074-3.

[12] Prabhakar P, Waas AM. Interaction between kinking and splitting in the compressive failure of unidirectional fiber reinforced laminated composites. Compos Struct 2013;98:85–92. https://doi.org/10.1016/j.compstruct.2012.11.005.

[13] Kyriakides S, Arseculeratne R, Perry EJ, Liechti KM. On the compressive failure of fiber reinforced composites. Int J Solids Struct 1995;32:689–738. https://doi.org/10.1016/0020-7683(94)00157-R.

[14] Wang X, Guan Z, Liu N, Zhang M, Li Z, Meng Q, et al. A 3D micromechanics-based failure criterion for fiber reinforced composites under longitudinal compression. Compos Part A Appl Sci Manuf 2022;161:107076. https://doi.org/10.1016/J.COMPOSITESA.2022.107076.

[15] Díaz-Montiel P, Venkataraman S, Kim H. The effects of plasticity mechanisms on micromechanics of composites with fiber waviness defects under compression. Doi: 10.1080/15376494.2021.2001121.

[16] Hyde A, He J, Cui X, Lua J, Liu L. Effects of microvoids on strength of unidirectional fiber-reinforced composite materials. Compos B Eng 2020;187:107844. https://doi.org/10.1016/J.COMPOSITESB.2020.107844.

[17] Mehdikhani M, Petrov NA, Straumit I, Melro AR, Lomov SV, Gorbatikh L. The effect of voids on matrix cracking in composite laminates as revealed by combined computations at the micro- and meso-scales. Compos Part A Appl Sci Manuf 2019;117:180–92. https://doi.org/10.1016/J.COMPOSITESA.2018.11.009.

[18] Taherzadeh M, Baghani M, Baniassadi M, Abrinia K, Safdari M. Modeling and homogenization of shape memory polymer nanocomposites. Compos B Eng 2016;91:36–43. https://doi.org/10.1016/J.COMPOSITESB.2015.12.044.

[19] Jarali CS, Madhusudan M, Vidyashankar S, Raja S. A new micromechanics approach to the application of Eshelby's equivalent inclusion method in three phase composites with shape memory polymer matrix. Compos B Eng 2018;152:17–30. https://doi.org/10.1016/J.COMPOSITESB.2018.06.028.

[20] Fedotov AF. Mori-Tanaka experimental-analytical model for predicting engineering elastic moduli of composite materials. Compos B Eng 2022;232:109635. https://doi.org/10.1016/J.COMPOSITESB.2022.109635.

[21] Vignoli LL, Savi MA, Pacheco PMCL, Kalamkarov AL. Micromechanical analysis of transversal strength of composite laminae. Compos Struct 2020;250:112546. https://doi.org/10.1016/J.COMPSTRUCT.2020.112546.

[22] Sharma A, Daggumati S, Gupta A, Van Paepegem W. On the prediction of the bi-axial failure envelope of a UD CFRP composite lamina using computational micromechanics: Effect of microscale parameters on macroscale stress–strain behavior. Compos Struct 2020;251:112605. https://doi.org/10.1016/J.COMPSTRUCT.2020.112605.

[23] Tang H, Chen Z, Xu H, Liu Z, Sun Q, Zhou G, et al. Computational micromechanics model based failure criteria for chopped carbon fiber sheet molding compound composites. Compos Sci Technol 2020;200:108400. https://doi.org/10.1016/J.COMPSCITECH.2020.108400.

[24] Drugan WJ, Willis JR. A micromechanics-based nonlocal constitutive equation and estimates of representative volume element size for elastic composites. J Mech Phys Solids 1996;44:497–524. https://doi.org/10.1016/0022-5096(96)00007-5.

[25] Bargmann S, Klusemann B, Markmann J, Schnabel JE, Schneider K, Soyarslan C, et al. Generation of 3D representative volume elements for heterogeneous materials: a review. Prog Mater Sci 2018;96:322–84. https://doi.org/10.1016/J.PMATSCI.2018.02.003.

[26] Kanit T, Forest S, Galliet I, Mounoury V, Jeulin D. Determination of the size of the representative volume element for random composites: statistical and numerical approach. Int J Solids Struct 2003;40:3647–79. https://doi.org/10.1016/S0020-7683(03)00143-4.

[27] Naya F, Herráez M, Lopes CS, González C, Van der Veen S, Pons F. Computational micromechanics of fiber kinking in unidirectional FRP under different environmental conditions. Compos Sci Technol 2017;144:26–35. https://doi.org/10.1016/j.compscitech.2017.03.014.

[28] He C, Ge J, Cao X, Chen Y, Chen H, Fang D. The effects of fiber radius and fiber shape deviations and of matrix void content on the strengths and failure mechanisms of UD composites by computational micromechanics. Compos Sci Technol 2022;218:109139. https://doi.org/10.1016/J.COMPSCITECH.2021.109139.

[29] Li B, Zhao M, Wan X. The influence of void distribution on transverse mechanical properties of unidirectional composites. In: 2017 8th International Conference on Mechanical and Aerospace Engineering, ICMAE 2017 2017:209–14. Doi: 10.1109/ICMAE.2017.8038644.

[30] Wan L, Ismail Y, Zhu C, Zhu P, Sheng Y, Liu J, et al. Computational micromechanics-based prediction of the failure of unidirectional composite lamina subjected to transverse and in-plane shear stress states. J Compos Mater 2020;54:3637–54.

[31] Chen J, Wan L, Ismail Y, Hou P, Ye J, Yang D. Micromechanical analysis of UD CFRP composite lamina under multiaxial loading with different loading paths. Compos Struct 2021;269:114024. https://doi.org/10.1016/J.COMPSTRUCT.2021.114024.

[32] Chen J, Wan L, Ismail Y, Ye J, Yang D. A micromechanics and machine learning coupled approach for failure prediction of unidirectional CFRP composites under triaxial loading: A preliminary study. Compos Struct 2021;267:113876. https://doi.org/10.1016/J.COMPSTRUCT.2021.113876.

[33] Ismail Y, Yang D, Ye J. Discrete element method for generating random fibre distributions in micromechanical models of fibre reinforced composite laminates. Compos B Eng 2016;90:485–92. https://doi.org/10.1016/J.COMPOSITESB.2016.01.037.

[34] Sun Q, Zhou G, Meng Z, Guo H, Chen Z, Liu H, et al. Failure criteria of unidirectional carbon fiber reinforced polymer composites informed by a computational micromechanics model. Compos Sci Technol 2019;172:81–95. https://doi.org/10.1016/j.compscitech.2019.01.012.
[35] Gitman IM, Askes H, Sluys LJ. Representative volume: Existence and size determination. Eng Fract Mech 2007;74:2518–34. https://doi.org/10.1016/J.ENGFRACMECH.2006.12.021.
[36] Okereke MI, Akpoyomare AI. A virtual framework for prediction of full-field elastic response of unidirectional composites. Comput Mater Sci 2013;70:82–99. https://doi.org/10.1016/J.COMMATSCI.2012.12.036.
[37] Kanit T, N'Guyen F, Forest S, Jeulin D, Reed M, Singleton S. Apparent and effective physical properties of heterogeneous materials: Representativity of samples of two materials from food industry. Comput Methods Appl Mech Eng 2006;195:3960–82. https://doi.org/10.1016/J.CMA.2005.07.022.
[38] Chen G, Ozden UA, Bezold A, Broeckmann C. A statistics based numerical investigation on the prediction of elasto-plastic behavior of WC–Co hard metal. Comput Mater Sci 2013;80:96–103. https://doi.org/10.1016/J.COMMATSCI.2013.04.004.
[39] Fiedlera B, Hojo M, Ochiai KS, Schulte MA. Failure behavior of an epoxy matrix under different kinds of static loading 2001;61:1615–24.
[40] Dassault Systèmes. Abaqus 6.13 documentation; 2013 n.d.
[41] Lubliner J, Oliver J, Oller S, Oñate E. A plastic-damage model for concrete. Int J Solids Struct 1989;25:299–326. https://doi.org/10.1016/0020-7683(89)90050-4.
[42] Lee J, Fenves GL. Plastic-damage model for cyclic loading of concrete structures. J Eng Mech 1998;124:892–900.
[43] Turon A, Camanho PP, Costa J, Dávila CG. A damage model for the simulation of delamination in advanced composites under variable-mode loading. Mech Mater 2006;38:1072–89. https://doi.org/10.1016/J.MECHMAT.2005.10.003.
[44] Ismail Y, Wan L, Chen J, Ye J, Yang D. An ABAQUS® plug-in for generating virtual data required for inverse analysis of unidirectional composites using artificial neural networks. Eng Comput 2022;38:4323–35. https://doi.org/10.1007/S00366-021-01525-1/TABLES/6.
[45] Jiang H, Ren Y, Liu Z, Zhang S. Microscale finite element analysis for predicting effects of air voids on mechanical properties of single fiber bundle in composites. J Mater Sci 2019;54:1363–81. https://doi.org/10.1007/s10853-018-2928-6.
[46] Dong J, Huo N. A two-scale method for predicting the mechanical properties of 3D braided composites with internal defects. Compos Struct 2016;152:1–10. https://doi.org/10.1016/J.COMPSTRUCT.2016.05.025.
[47] Wang Y, Burnett TL, Chai Y, Soutis C, Hogg PJ, Withers PJ. X-ray computed tomography study of kink bands in unidirectional composites. Compos Struct 2017;160:917–24. https://doi.org/10.1016/J.COMPSTRUCT.2016.10.124.
[48] Nelms K, Paul PP, Wowogno A, Chen Y, Lukic B, Rack A, et al. Effects of fibre orientation on compression micromechanics in CFRP investigation by computed tomography. In: Twenty-third international conference on composite materials (ICCM23), Belfast, Aug, 2023.
[49] Lemanski SL, Sutcliffe MPF. Compressive failure of finite size unidirectional composite laminates with a region of fibre waviness. Compos Part A Appl Sci Manuf 2012;43:435–44. https://doi.org/10.1016/J.COMPOSITESA.2011.11.007.
[50] Lee J, Soutis C. A study on the compressive strength of thick carbon fibre–epoxy laminates. Compos Sci Technol 2007;67:2015–26. https://doi.org/10.1016/J.COMPSCITECH.2006.12.001.
[51] Ploeckl M, Kuhn P, Grosser J, Wolfahrt M, Koerber H. A dynamic test methodology for analyzing the strain-rate effect on the longitudinal compressive behavior of fiber-reinforced composites. Compos Struct 2017;180:429–38.
[52] Camanho PP, Maimí P, Dávila CG. Prediction of size effects in notched laminates using continuum damage mechanics. Compos Sci Technol 2007;67:2715–27. https://doi.org/10.1016/J.COMPSCITECH.2007.02.005.
[53] Gutkin R, Pinho ST, Robinson P, Curtis PT. Micro-mechanical modelling of shear-driven fibre compressive failure and of fibre kinking for failure envelope generation in CFRP laminates. Compos Sci Technol 2010;70:1214–22. https://doi.org/10.1016/j.compscitech.2010.03.009.
[54] Gutkin R, Pinho ST, Robinson P, Curtis PT. On the transition from shear-driven fibre compressive failure to fibre kinking in notched CFRP laminates under longitudinal compression. Compos Sci Technol 2010;70:1223–31. https://doi.org/10.1016/J.COMPSCITECH.2010.03.010.